Hindawi
Advances in Civil Engineering
Volume 2020, Article ID 8817112, 14 pages
https://doi.org/10.1155/2020/8817112

Research Article

Prototype Experimental Investigation of the Failure Mechanism and Crack Propagation of Segment Lining for Staggered Jointed Assembly

Songyu Cao,[1] **Kun Feng**,[1] **Xun Liu**,[1] **Mingqing Xiao**,[2] **Chuan He**,[1] **and Ce Li**[3]

[1]*Key Laboratory of Transportation Tunnel Engineering, Ministry of Education, Southwest Jiaotong University, Chengdu 610031, China*
[2]*China Railway Siyuan Survey and Design Group Co. Ltd., Wuhan, Hubei 430071, China*
[3]*National & Local Joint Engineering Research Center of Underwater Tunnel Technology, Wuhan, Hubei 430071, China*

Correspondence should be addressed to Kun Feng; kfeng123@163.com

Received 27 September 2020; Revised 1 December 2020; Accepted 16 December 2020; Published 24 December 2020

Academic Editor: bingxiang yuan; yuanbx@gdut.edu.cn

In order to ascertain the failure characteristics of a segment structure with distributed mortises and tenons, one should be aware of the rules of key parameters and the development of cracks during the failure process. In this paper, based on the Foguan-Guangcheng Intercity Railway Tunnel Project, a prototype test of the structure of a segment with a staggered joint assembly was performed to study the local mechanical characteristics of the segment lining of the vault. The main conclusions were as follows: (1) The failure process in the test was classified as large eccentric compression failure, and the bearing capacity limit was $M = 1993$ kN m. (2) The overall displacement distribution of the segment structure was funnel-shaped, and the failure process was divided into three stages, that is, the elastic stage, the elastoplastic stage, and the plastic stage. Thus, it is recommended that the index of the single-point displacement limit of this tunnel be reduced appropriately to be between 1.5 and 1.8%. (3) The change rule of the longitudinal joint opening of the segment can be divided into three stages, that is, slow increase, accelerated increase, and sharp increase. For normal use, the limit of the opening of the longitudinal joint is set at 3 mm. (4) The width of the structural crack and the vertical displacement of the control section can be used as the safety evaluation index of this project. When either a large increase in the width of the crack occurs or the displacement specified above is reached, it can be considered that the structure is about to fail, and immediate protective measures must be taken.

1. Introduction

In the utilization of underground space for urban public transportation, shield construction has been used extensively because of its advantages, which include low environmental impact, a high degree of mechanization, safe and fast construction, and no limitations due to topography or geomorphology. As a result, the shield method [1–3] has become the main approach for constructing tunnels. However, this method usually causes uneven settlement in the longitudinal direction of the tunnel when passing through composite strata during construction, which is manifested by large settlement and dislocation of the lining of the segment. Specifically, the settlement and the value of the internal force of the vault generally are greater than the bottom and the waist of the arch [4], and the same problem also occurs when the tunnel passes through a lateral composite stratum [5]. It is apparent that the vault segment is the weak link in the design when passing through the composite stratum. Therefore, it is necessary to conduct an original loading test of the structure of the segment to explore the factors and laws that potentially could affect the mechanical properties of the vault segment in the composite stratum. As a matter of fact, design experience can be provided, and structural safety can be ensured. Segments are the most basic structural unit of a shield tunnel, and they are damaged frequently during construction and operation. A damaged segment poses a serious threat to the operational safety of a

shield tunnel, so many scholars have conducted extensive research on the characteristics of damaged segments.

He et al. conducted a prototype test of shield segments, and the distribution law of the internal force for the segment ring was analyzed and compared with the numerical calculations based on the Guangzhou-Shenzhen-Hong Kong Shiziyang Tunnel [6]. Yan et al. conducted prototype tests of the joints of the segment, and they studied the rotation stiffness of the longitudinal joints under positive and negative bending moments [7]. Qiu et al. compared and analyzed the differences in the mechanical behaviors of single segments and assembled segments in the staggered joint assembly, and they proved the influential rule for the axial compression ratio, eccentricity, and bolt pretension [8]. Kun et al. explored the mechanism of the shield tunnel assembly effect, and they discussed the influence of the longitudinal force on the internal force of the structure of the segment through theoretical analysis and a loading test [9, 10].

In terms of the analysis of the structural failure of the segments, He et al. conducted a series of prototype tests using different assembly methods for segment lining based on the Guangzhou-Shenzhen-Hong Kong Shiziyang Tunnel, and they discussed the structural and mechanical properties [11]. Qiu et al. conducted a failure test using a prototype segment to investigate the effect on the assembly of the staggered joint segment, and they explored the cracking time, the process of the development of cracks in the structure, the stress and deformation of the structure, and the joint opening [12]. Kun et al. conducted a loading test of a prototype segment of the Nanjing Yangtze River Tunnel to provide the engineering background they needed, and they discussed the failure mode of the lining of the segment due to the high water pressure [13]. Liang et al. conducted a series of prototype tests of assembled segments subjected to high water pressure conditions and demonstrated the mechanical properties [14]. Xia studied the overall internal force law and failure characteristics of a segment structure for different water and soil pressures during construction based on the Shiziyang Tunnel in Guangzhou [15]. Xiangli et al. conducted full-scale tests of single segments to simulate the upper stacking effect, and they analyzed the overall stress process, the failure mode, and the ultimate bearing capacity of the segment [16]. Ye et al. conducted a full-scale static load test on the shield tunnel segment, and they described the deformation of the segment, cracks, joint openings, and the development and failure process of the stress on the bolts during the test. They also conducted a detailed investigation of the load-bearing process [17]. Lu comprehensively used a variety of research methods, such as field investigations, tests of similar models, numerical simulation, and field tests, to study the influence of the construction load on the mechanical characteristics of the structure for the segment lining, and he determined the distribution of the cracks in the segment lining for different jack-thrust conditions [18]. Wang et al. conducted similar model tests based on the Shiziyang shield tunnel project crossing Guangzhou, Shenzhen, and Hong Kong. They compared and analyzed the internal force, deformation, acoustic emission data, and crack-development law of a segment structure for different water pressure conditions [19]. Wang et al. used similar model test methods to compare and analyze the influence of different segment assemblies on the failure characteristics of segment lining structures [20]. Bloomberg used similar model tests combined with finite element model numerical calculations to study systematically the progressive failure mechanism and failure process of the segments of shield tunnels, and he identified the different factors involved in the progressive failure of segments in the structures of underwater shield tunnels [21]. Yang and Xie used the finite element calculation method based on fracture mechanics to discuss the mechanisms for single segment, combined segments, and entire ring segments [22].

In summary, numerical analysis and model tests are used mostly for the research of segment linings, but those methods are limited. Crucial parameters such as crack propagation and the failure process cannot be observed specifically, and, as a matter of fact, it is important to conduct a prototype test to directly present the failure mechanism and crack propagation of the segment lining. In addition, several prototype tests are conducted to investigate the mechanical properties of the segment lining, but, as shown in Figure 1(b), full-ring mortises and tenons are used mostly for the connection between segment rings for prototype tests, while the failure process of segments with distributed mortises and tenons is rarely analyzed. Therefore, as shown in Figure 1(a), based on the Foguan-Shiziyang tunnel project, the self-developed "multi-functional shield tunnel structure test system" was used to conduct the prototype failure test of segments with distributed mortises and tenons considering the staggered joint assembly. The mechanical properties and the crack propagation law were studied comprehensively and the evaluation of segment failure was provided.

2. Design of the Test

2.1. Objective of the Test. The "shield tunnel segment loading" device is used in this paper, and the loading capacity of the device is 5000 kN in both the vertical and horizontal directions. The device can be used to determine the bending, shear, and joint mechanical properties of the shield tunnel with a maximum diameter of 16 m. As presented in Figures 2(a) and 2(b), the test device consists of a large-scale test bench, horizontal and vertical jacks, load distribution beams, pressure beams, rotating hinge supports, consoles, and steel box beam bases that provide reaction forces to form a self-reaction system. In the vertical direction, the load is transferred sequentially to the load distribution beam through the vertical jack. The left and right ends of the test piece are carried by rotating hinge supports, and the test segment can be rotated freely at both ends.

The main structure of the tunnel for the Foguan-Guangcheng Intercity Railway Tunnel Project consists of a C60, single-layer assembled, reinforced, concrete segment lining based on the "1 + 2 + 6" block method, that is, 1 key block (the F block), 2 adjacent blocks (the L1 block and the L2 block), and 6 standard blocks (blocks B1–B6). The outer diameter is 13.1 m, the inner diameter is 12.0 m, the width is

(a) (b)

Figure 1: Circumferential joint. (a) Distributed mortises and tenons. (b) Full-ring mortises and tenons.

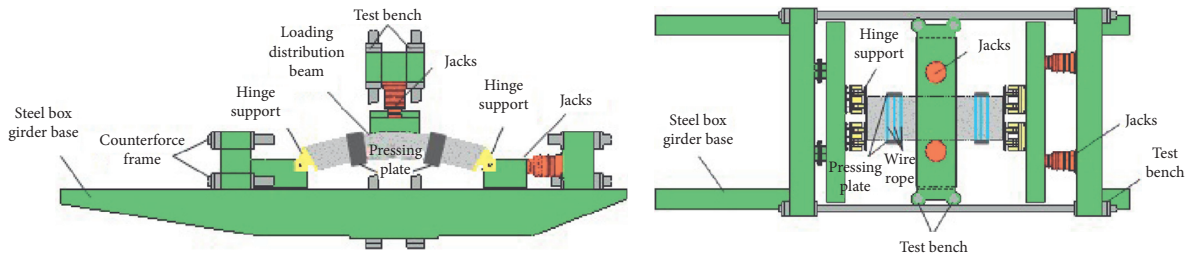

(a) (b)

Figure 2: 3D schematic diagram of segment loading. (a) Front view of the structure; (b) top view of the structure.

2 m, and the thickness is 0.55 m. There are a total of 24 circumferential bolts in the structure of the segment, and there are 34 longitudinal bolts between the rings, as shown in Figure 3. Four pairs of distributed mortises and tenons are used for the circumferential joint.

2.2. Test Specimen and the Layout of the Measuring Point. As presented in Figure 4, two sets of three-ring, combined-segment test pieces were used in the experiment. B1 and B2 are the adjacent ring blocks, and B3 is the middle block.

The parameters measured in the experiment were internal force, vertical displacement, concrete strain of the segment structure, and the joint opening. These measurements were performed by a differential displacement sensor with an accuracy of 0.01 mm. The layout of the measuring points is shown in Figure 5. Due to the elasticity of concrete, uneven displacement occurs in horizontal and longitudinal direction frequently; to more accurately analyze the segment deformation, a series of displacement gauges were arranged equidistantly on the arc surface of the vault for the middle segment and each adjacent segment ring; the chord length is shown in Figure 3. Three sets of displacement slot meters are placed equidistantly for the observation of circumferential joint openings, while two more slot meters are used for longitudinal joint openings.

2.3. Test Loading Plan. In order to achieve the ultimate bearing capacity of the segment, it was necessary to choose a large eccentricity. Therefore, the eccentricity was selected to be 0.35 m in the normal loading stage and the failure stage for this test, and the maximum axial compression ratio was 0.1. The loading conditions were as follows:

(1) Eccentricity is maintained constant in the normal loading stage, and the horizontal and vertical loads are applied gradually. The horizontal jack was loaded to 0.4 MPa per level, and the corresponding horizontal force was 50 kN per level. The load was increased gradually until the load on the horizontal jack reached 4725 kN and $\lambda = 0.1$.

(2) The axial force was kept constant in the failure stage. Only the force of the vertical jack was increased, that is, to 0.4 MPa per level, and the corresponding vertical force was increased by 50 kN. The load was increased gradually until the vertical displacement of the structure entered the platform stage, and, finally, the structure was damaged and failed.

Figure 6 shows the change law of the thrusts of the horizontal and vertical jack loads and the internal force as the load increases. In the normal load stage, as the load of the vertical jack increases, the axial force and bending moment of the segment control section also increase gradually. During the second stage of loading, as the vertical load increases continuously, the eccentricity of the section increases rapidly, which leads to a significant increase in the bending moment of the control section. Thus, the structural deformation increases, and, as a consequence, the structure of the segment finally reaches its bearing limit.

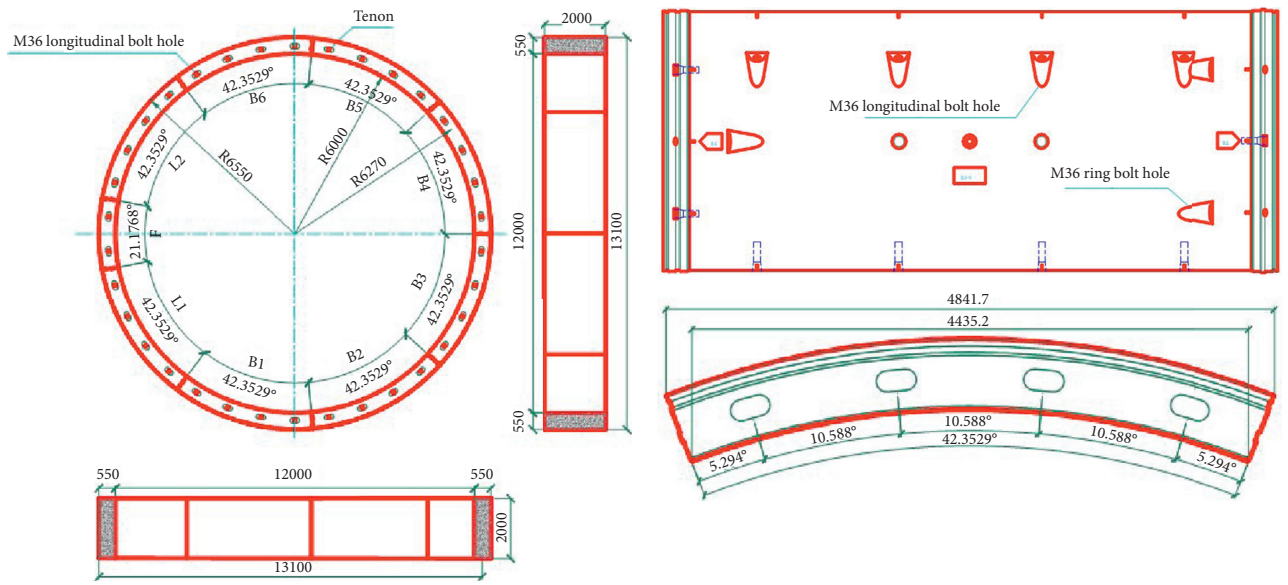

Figure 3: Diagram of the segment structure (mm). (a) Schematic diagram of the segments; (b) schematic of the detailed segment structure.

Figure 4: Test device.

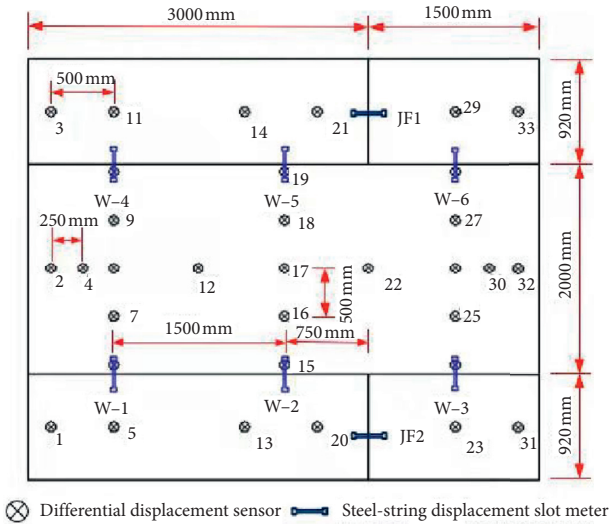

Figure 5: Layout of the measured points.

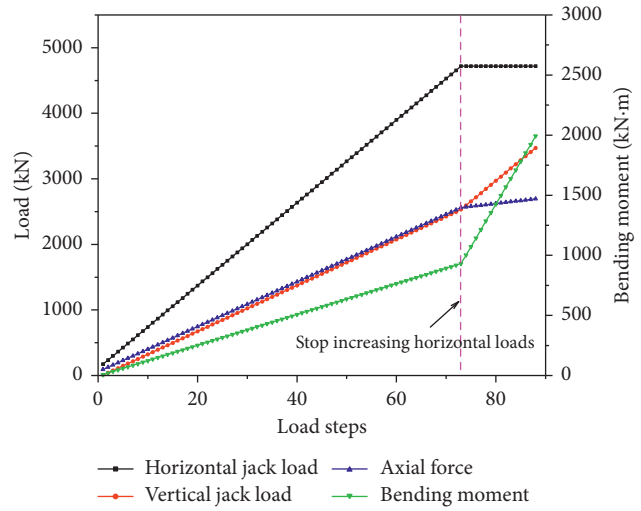

Figure 6: Test loading process.

3. Study of the Mechanical Properties of Segments in the Failure Stage

3.1. Structural Internal Force Characteristics. The bearing capacity of the segment structure is evaluated through the section stress, and, commonly, the segment bearing capacity is evaluated by the bearing capacity curve. The section bearing capacity curve can be determined by the relevant parameters, such as the grade of the concrete, the strength of the reinforcing steel, the thickness of the protective layer, the size of the segment, and the amount of reinforcement. The test object is a segment of the Foguan-Shiziyang Tunnel project, which used a C50-reinforced concrete structure; the

design value of tensile strength was $f_t = 1.89$ MPa, and the design value of the compressive strength was $f_c = 23.1$ MPa; the internal steel bar was HRB400. The thickness of the protective layer was 55 mm, the width of the segment was 2 m, and the thickness of the segment was 0.55 m. According to the design parameters above, the bearing capacity curve of the main section of the segment was calculated according to the eccentric compression of the reinforced concrete structure, as shown in Figure 7.

The N-M curve of the main structure for the segment shows that as the axial force increased, the bending moment increased first and then decreased. The inside of the curve is defined as the safe area, while the outside of the curve is the failure area. As presented in Figure 6, the Pa point is presented as the axial compression failure; the bending moment at this position is equal to 0, the axial force reaches its maximum value, and the ultimate axial force is 29,800 kN; the Pc point is pure bending failure, and the Pb point is the maximum bending moment, and the ultimate bending moment is 2,708 kN m, which is the boundary failure. The other locations are compression-bending failures. The PaPb section is damaged by the small, eccentric compression. As the axial force increases, the bearing capacity of the bending moment of the section becomes smaller, and the PbPc section is damaged under large eccentric compression. As the axial force increases, the bending moment bearing capacity of the section becomes larger [23].

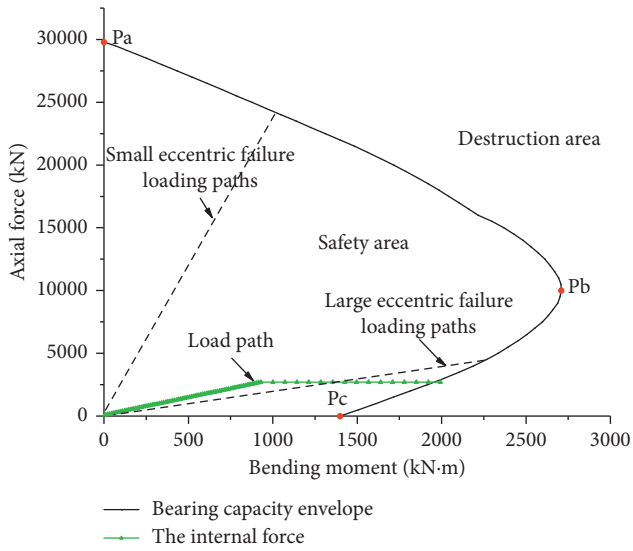

Figure 7: N-M curve for control section.

3.2. Structural Deformation Characteristics. Figure 8 shows the overall vertical displacement for different ratios of the bending moment to the failure load of the intermediate ring of the combined segments. For the vertical axis, 6000 mm is the radius of the segment ring. The vertical displacement of the structure gradually increases as the load ratio increases. When the load ratio is small, the overall settlement of the segment follows a funnel-shaped distribution; that is, the vertical displacement in the middle of the segment is large, and the displacement on both sides is small. The difference in the displacement within the vault (85°–95°) is obvious. The left and right vertical displacements of the segments are asymmetrical, and the vertical displacement of the jack loading side is slightly larger than that of the horizontal fixed support side. As the load ratio increases, the vertical displacement in the middle of the structure increases faster, and it had reached 45.65 mm when the structure failed.

In the process of the construction and operation of a tunnel, deformation is the key factor to control the overall stress of the segment. The maximum displacement of a single point up to 2‰ of the diameter of the segment often is used as the limiting index [24]. Figure 8 shows that nine measuring points were selected for the segment at different positions along the ring direction of the segment.

As presented in Figure 9, the maximum displacement of a single point at the position of each measuring point increases as the vertical load increases. Basically, the growth law can be divided into three stages. In the first stage, from a vertical load of 0 kN to a vertical load of 2721 kN, the single-point displacement of each measuring point increases linearly, and this stage is defined as the elastic stage. After the vertical load reaches 2721 kN, the increase in the vertical displacement of each measuring point accelerates, and the inflection point appears. This stage is defined as the elastic-plastic stage. When the failure load is reached, the vertical displacement of each measuring point continues to increase even though loading has been stopped, and the segment

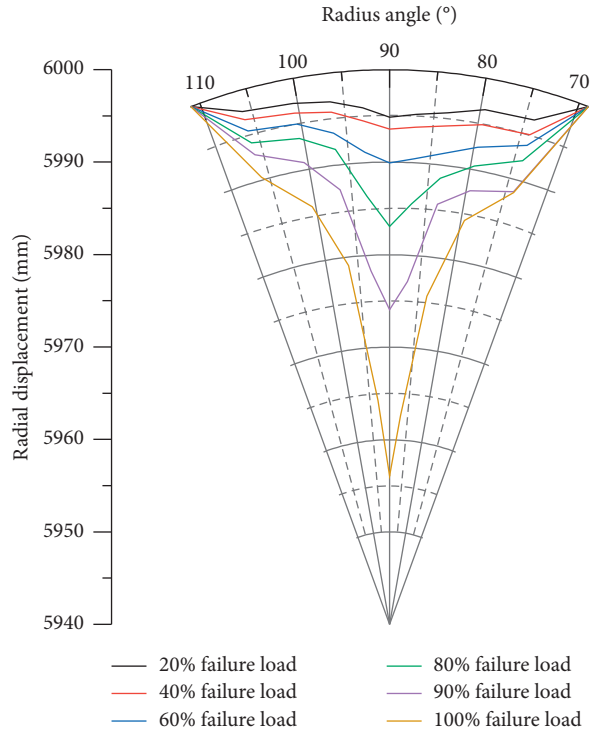

Figure 8: The overall vertical displacements for different ratios of the bending moment to the failure load of the intermediate ring of the combined segments.

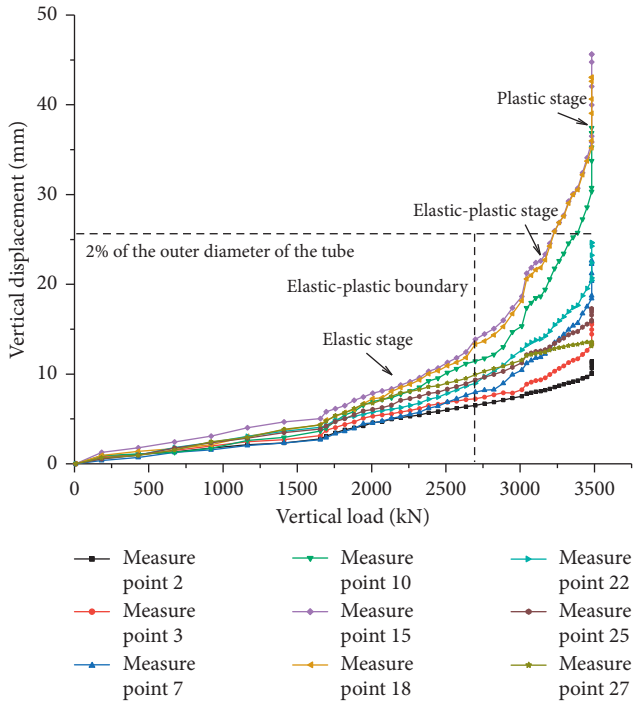

Figure 9: Change in the single-point displacement of each measuring point for different vertical loads.

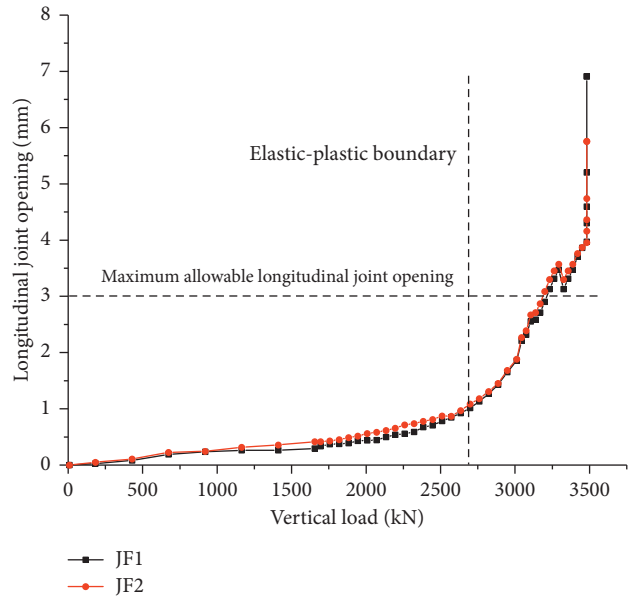

Figure 10: Variation law of longitudinal joint opening for different vertical loads.

becomes unstable. This stage is defined as the plastic stage. According to the limit index of the single-point maximum displacement of 2% in the failure state, the maximum vertical displacement of the vault reaches 45.1 mm, which is 3.5% of the outer diameter of the segment. In the elasto-plastic stage, only three vertical displacements reach the limit index, that is, measuring point 15 (the vault position), measuring point 10 (close to the left side of the vault), and measuring point 18 (close to the right side of the vault), and the proportion of the corresponding load (2% of the diameter) to the failure load is about 90%. In other words, when the displacement reaches the limit index, the segment is about to approach the limit of its bearing capacity. Thus, it is apparent that, for the segments with distributed mortises and tenons, it would be dangerous to use a single-point displacement of 2% as the deformation limit index to guarantee the displacement inside the elastic-plastic stage, and the increase in the slope of the displacement is relatively small, and it can be reduced appropriately to the range of 1.5% to 1.8%.

3.3. Characteristics of Joint Opening. In this test, all of the circumferential joints of the segment were open on the inside and closed on the outside, and the amount of opening was greater than the amount of closing. According to related research [25], the maximum opening of the shield tunnel segment joint is 3 mm in the normal use stage, while the maximum opening of the ring joint in this test is only 0.29 mm, which is far from the limit. However, the longitudinal joint has a large opening, and it is necessary to study the corresponding development law. Figure 10 shows the change law of the amount of opening for the two longitudinal joints for different vertical loads.

The longitudinal joint opening increases as the load ratio increases. It also can be divided into three stages, i.e., slow increase, accelerated increase, and sharp increase. The first stage is the slow increase stage (in which the vertical load is in the range of 0–2,721 kN). When a small load is applied, the longitudinal joint opening of the segment develops slowly, showing a linear growth trend. At the end of this stage, the longitudinal joint openings of JF1 and JF2 on both sides of the combined segment are 1.1 mm. Generally speaking, the development of longitudinal joint openings at this stage is relatively stable, and the value is also small.

The second stage is the accelerated increase stage, in which the vertical load is in the range of 2721 to 3482 kN. When the applied load increases gradually, the openings of the longitudinal joints of JF1 and JF2 accelerate, and the growth rates of the longitudinal joint openings continue to increase. When the vertical load was at 3,294 kN, the longitudinal joint opening suddenly decreased and then immediately resumed its linear growth. This may have been related to the severe dislocation between the segments when the damage was developing and the mortises and tenons in circumferential joint also were damaged. When the failure load was reached, the openings of the longitudinal joints of JF1 and JF2 were 3.971 mm and 3.955 mm, respectively.

The third stage is a sharp increase stage, and the failure load is unchanged. After the load is stopped, the longitudinal joint openings of JF1 and JF2 increase sharply, and the segment is in the unstable stage. The final openings of the two longitudinal openings were 6.9 mm and 5.7 mm, respectively. Compared with the maximum opening amount of 3.9 mm in the second stage, the amounts of the openings of the longitudinal joints in this stage increased by 2.9 mm

and 1.8 mm, respectively. The growth rates accounted for 42.6% and 31.4% of the total openings, respectively. After the ultimate state of the load-bearing capacity of the segment, the opening of the longitudinal joint still increased significantly.

When the opening of the two joints reached the normal use specification value of 3 mm, the vertical load that was being applied was 3,199 kN. At this time, the bending moment of the segment accounted for 87.5% of the failure moment. After reaching the normal use specification value, the segment still has a certain safety margin, so it is more reasonable to set the longitudinal joint opening limit under normal use as 3 mm.

3.4. Rebar Strain Characteristics. The inner steel bar of the segment is under tension, the steel bar of the outer side is compressed, and the maximum tensile strain of the steel bar occurs at the position of the middle ring vault. The maximum tensile strain of the inner main reinforcement was 2023 $\mu\varepsilon$. The type of steel used in this test was HRB400, and the corresponding yield strain was 1904 $\mu\varepsilon$. Therefore, the inner main reinforcement of the middle target segment in this failure test yielded, and the other positions had small strains but had not reached yield status. The maximum compressive strain of the outer main reinforcement was −844 $\mu\varepsilon$, which was less than the yield state. Therefore, the tensile strain and compressive strain of the steel bar at the position of the vault were selected to analyze the change law of the vertical load, as shown in Figure 11. The process for the variation of the stress of the inner main reinforcement of the middle target segment basically can be divided into two stages, that is, a linear change and a nonlinear change. When the vertical load is small, the strain of the steel bar basically changes linearly as the vertical load increases. As the vertical load continues to increase and reaches about 2500 kN, the strain of the steel bar begins to show the characteristics of nonlinear growth, and the growth rate increased significantly compared with the first stage. When the vertical load was 3325 kN, the main reinforcement reached the yield strain. When the outer main reinforcement for the segment of the middle ring was compressed, the change law of compressive strain was different from the law of tensile strain. With the increase of the vertical load, the strain of the steel bar basically followed the linear growth law. The maximum compressive strain of −844 $\mu\varepsilon$ occurred at the failure load, but the value of the compressive strain was small and had not yet reached the yield strain.

4. Analysis of the Failure Process of the Segment Structure

In order to study the local failure characteristics of the segment structure under the load of the vault, the cracking time of the segment of the vault, the law of crack development, and the final failure form were analyzed comprehensively, and the failure mechanism of the segment was derived from this, as occurs in actual engineering.

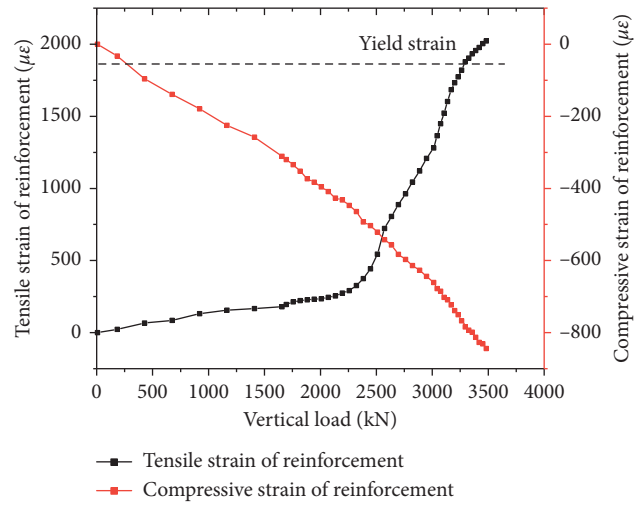

Figure 11: Strain of the main reinforcement at the vault position of the target segment of the middle ring.

4.1. Development of Cracks. During the test, the inner and outer surfaces of the arc of the middle ring of the assembled segments had different degrees of damage, but there was no damage to the adjacent rings. This was mainly due to the fact that the middle target segment was very rigid. The deformation of the segments was small, and the structure bore a large positive bending moment, which, in turn, caused the inner concrete to be under tension, and it finally reached the ultimate tensile strain and resulted in damage. However, due to the lessening of the stiffness of the longitudinal joints, the stiffnesses of the rings on both sides were small, and the ring bolts were oblique. The openings of the longitudinal joints were not constrained sufficiently. Under the combined influence of the factors, the segment rings on both sides can produce greater deformation without cracks. The failure process and the law of the development of cracks in the intermediate ring segment are illustrated in detail below. Figure 12 shows the process of the development of cracks in the arc for the segment.

Figure 13 shows the depths of the cracks in the thickness direction of the segment. When the vertical load reached 1901 kN, the first cracks appeared in the middle of the structure of the segment. There were 6 pieces of cracks, and the maximum length of the cracks was 708 mm, and the maximum width of the cracks was 0.1 mm. The direction of the cracks was along the width of the segment, so they are referred to as longitudinal cracks. These are one of the judging indicators of compression and bending failure, and they indicate that the structure is dominated by bending at this time. The positions of the cracks were distributed at the ring joints of the assembled segments, i.e., at the longitudinal edges of the B3 segment. The longitudinal cracks were asymmetrical, and the cracks at the upper edge were longer than the other cracks.

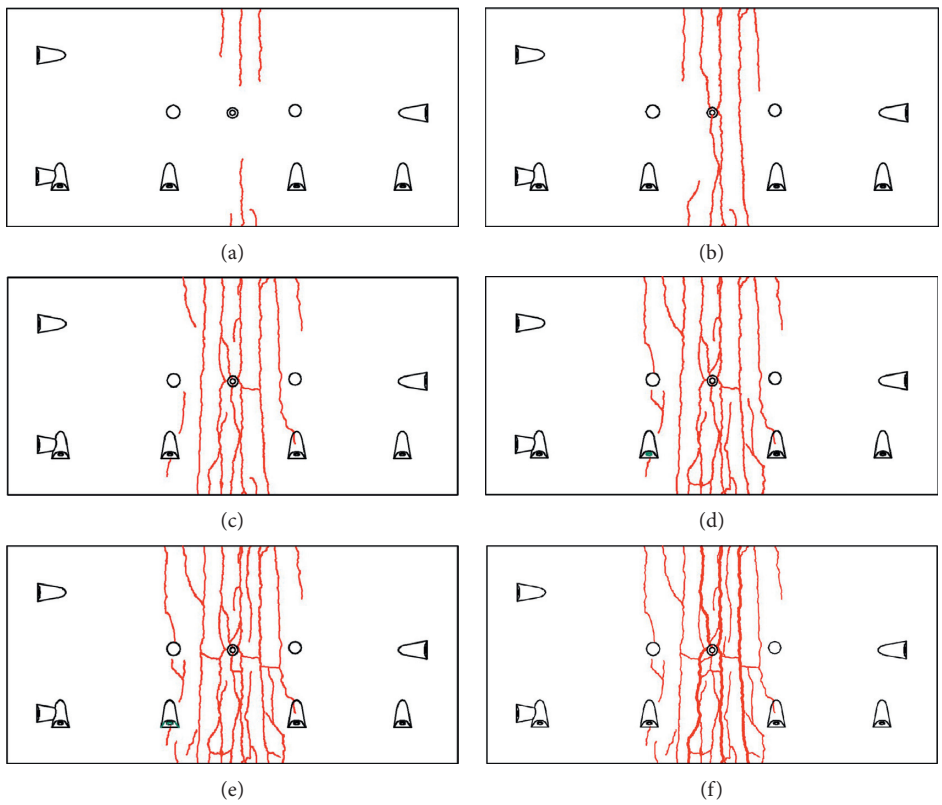

Figure 12: Development of cracks in the surface of the arc in the intermediate ring. (a) Vertical load = 1901 kN, (b) vertical load = 2182 kN, (c) vertical load = 2533 kN, (d) vertical load = 2784 kN, (e) vertical load = 3035 kN, and (f) failure load = 3482 kN.

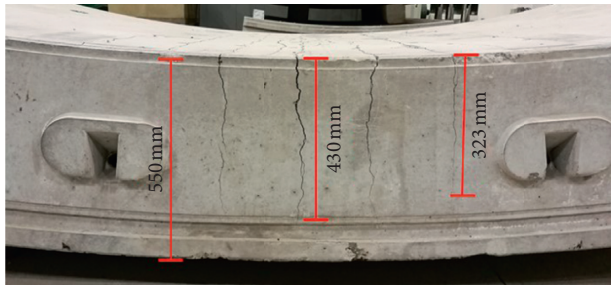

Figure 13: Result of crack development along the thickness direction.

When the vertical load reached 2182 kN, a second batch of cracks appeared in the middle of the structure of the segment, and cracks were generated at 7 new places. The maximum length of the cracks was 2,000 mm, and their maximum width was 0.21 mm. The first batch of 6 cracks gradually spread to the middle along the width direction, forming 3 parallel, penetrating cracks. The width of the main crack increased, and small, minor cracks were generated around it. All of the cracks were in the longitudinal direction; that is, no transverse cracks were found.

When the vertical load reached 2533 kN, the third batch of cracks appeared in the middle of the structure of the segment. Thirteen new cracks were generated, and the maximum length and width of the cracks were 2000 mm and 0.35 mm, respectively. Two new penetrating cracks occurred, and five main longitudinal cracks were formed. More secondary cracks were generated around the main crack, and it is worth noting that transverse cracks and diagonal cracks were generated between the main cracks. Cracks also appeared at the bolt holes and the positioning holes due to the concentration of stress at these locations, and there also was a tendency for cracks to develop in the bolt holes. There were more cracks in this stage in which the number of cracks developed most rapidly, but the increase in the widths of the cracks was small.

When the vertical load reached 2784 kN, the fourth batch of cracks appeared in the middle of the segment, and 9 new cracks occurred. The maximum length of the cracks was 2000 mm and their maximum width was 0.5 mm. The numbers of the secondary cracks and transverse cracks increased gradually. A new connecting crack was formed between the positioning hole and the edge of the segment. The rate of growth in the number of cracks was decreased.

When the vertical load reached 3035 kN, the fifth batch of cracks appeared in the middle of the structure, and one secondary crack and 3 transverse cracks were generated. The maximum length of the cracks was 2000 mm, and their maximum width was 1.5 mm.

When the vertical load reached 3223 kN, the sixth batch of cracks appeared in the middle of the structure, and two new diagonal cracks occurred. The maximum length of the cracks was 2000 mm, the maximum width of the main cracks

was 2.6 mm, and the maximum width of the secondary cracks was 1.9 mm.

As the vertical load continued to increase to 3482 kN, where it remained unchanged, no new cracks were generated, but the width of the main crack increased gradually, and the structure of the segment finally failed. The maximum width of the main crack was 5.4 mm. Only three cracks had widths greater than 5 mm.

Judging from the distribution of the cracks in the middle ring, the arc surface cracks in the segment mainly appeared in the vault position between the two positioning holes along the ring direction, and the first crack occurred in the edges. Most of the cracks were longitudinal cracks, and they had comparatively large widths, some of which exceeded 5 mm. The oblique cracks were narrower, and their angles relative to the longitudinal axis of the tunnel were between 0° and 45°. The least were the transverse cracks that occurred later between the longitudinal penetrating cracks along the direction of the segment ring.

Figure 13 shows the development of the middle ring B3 segment along the thickness direction, and it shows that the four longitudinal penetrating cracks with larger widths gradually had penetrated from the inner arc to the outer arc in the thickness direction of the segment. The shallowest depth of the cracks was 323 mm, which was 58.7% of the thickness of the segment; the deepest crack exceeded a depth of 430 mm, reaching 78.2% of the thickness of the segment. It was apparent that the segment had greater ductility in this failure, and the cracking depth was sufficient for the tensile steel bar inside the segment to fully exert its tensile strength, and the reinforcement of the segment was more reasonable, which is suitable for reinforcement failure. That is, when it is loaded to the final failure, the main reinforcement on the inner side of the segment bottom arch reaches the yielding state, and the segment is damaged in the section.

4.2. Final Failure State. When the segment finally failed, there were many cracks along the width direction on the surface of the arc of the middle ring segment structure vault. Among them, there were 5 parallel penetrating cracks, 3 cracks with widths of more than 5 mm, and 5.4 mm was the maximum width of a crack. In addition, there were a few diagonal and lateral cracks. Local compression and shear failure occurred at the left and right ends of the inner arc. The concrete at the top of the outer arc of the middle ring was crushed, and local compression-shear failure and cracks appeared near the longitudinal joints. Four longitudinal penetrating cracks with larger widths along the thickness of the segment gradually had extended from the inner arc to the outer arc in the thickness direction of the segment. The shallowest depth of the cracks was 323 mm, which was 58.7% of the thickness of the segment; the deepest crack exceeded the depth of 430 mm, reaching 78.2% of the thickness of the segment. The maximum opening of the longitudinal joint was 6.914 mm, the vertical displacement continued to increase to 45.65 mm, and the final failure form was compression-bending failure. Figure 14 shows the final broken shape of the segment. The mortises and tenons are damaged but not failed, the damage degrees of the mortises and tenons are different, and the middle tenons are damaged the most.

4.3. Analysis of the Mechanism of the Damage. The development of cracks on the inner arc had a greater impact on the load-bearing capacity of the structure of the segment. Thus, attention should be directed to the development of cracks on the inner arc during the construction and operation periods. Therefore, the characteristics of the development of cracks on the surface of the internal arc were analyzed in order to determine the failure mechanism. Figure 15 shows the rule concerning the development of cracks, including their numbers and widths. The law associated with the development of cracks in the surface of a segment of the arc and their widths is the opposite of the development law concerning the number of cracks. Thus, the change in the process of the development of cracks can be divided into two stages, that is, (1) the stage in which there is rapid growth in the number of cracks and (2) the stage in which the widths of the cracks increase rapidly. In the initial stage of loading, both the horizontal load and the vertical load are small, and the segment is not damaged. As the vertical load increases gradually, the bending moment of the segment also increases gradually. At this time, the structure of the segment is stretched on the surface of the inner arc. Small cracks began to appear where the stress was greater, and then the first batch of cracks quickly penetrated, forming several parallel cracks. Immediately afterwards, more cracks occurred around the main crack, and longitudinal cracks gradually appeared in other positions. At this stage, there were more cracks in the segment, and the growth rate was large, but the widths of the cracks developed slowly. After the continuous development of each secondary crack, there were connected transverse cracks between the longitudinal cracks, but there was a small number of them, and the width of the cracks increased rapidly at this stage.

In order to facilitate the analysis, five characteristic nodes were selected when the cracks were developing; that is, (1) the first visible cracks appeared on the arc surface of the segment, corresponding to node P1; (2) the first visible cracks penetrated, forming parallel and longitudinal cracks, and the maximum width reached the limit value of 0.2 mm in the use stage, corresponding to node P2; (3) the number of cracks increased the fastest, corresponding to node P3; (4) the widths of the cracks began to increase rapidly, corresponding to node P4; and, (5) finally, the segment failed, corresponding to node P5. The corresponding vertical loads for each node were 1901, 2182, 2533, 2784, and 3482 kN.

The development state of the cracks at the characteristic points P_1–P_5 in the figure and the relationship with the structural mechanical properties are shown in Table 1.

According to the results presented above, the process of the failure of the structure of the vault segment for the staggered joint assembly is as follows; that is, the deformation of the middle ring vault position increases ⟶ the visible micro cracks appear at the edge of the inner arc ⟶ the cracks of the inner arc continue to develop, and the through cracks (the width direction of the segment is

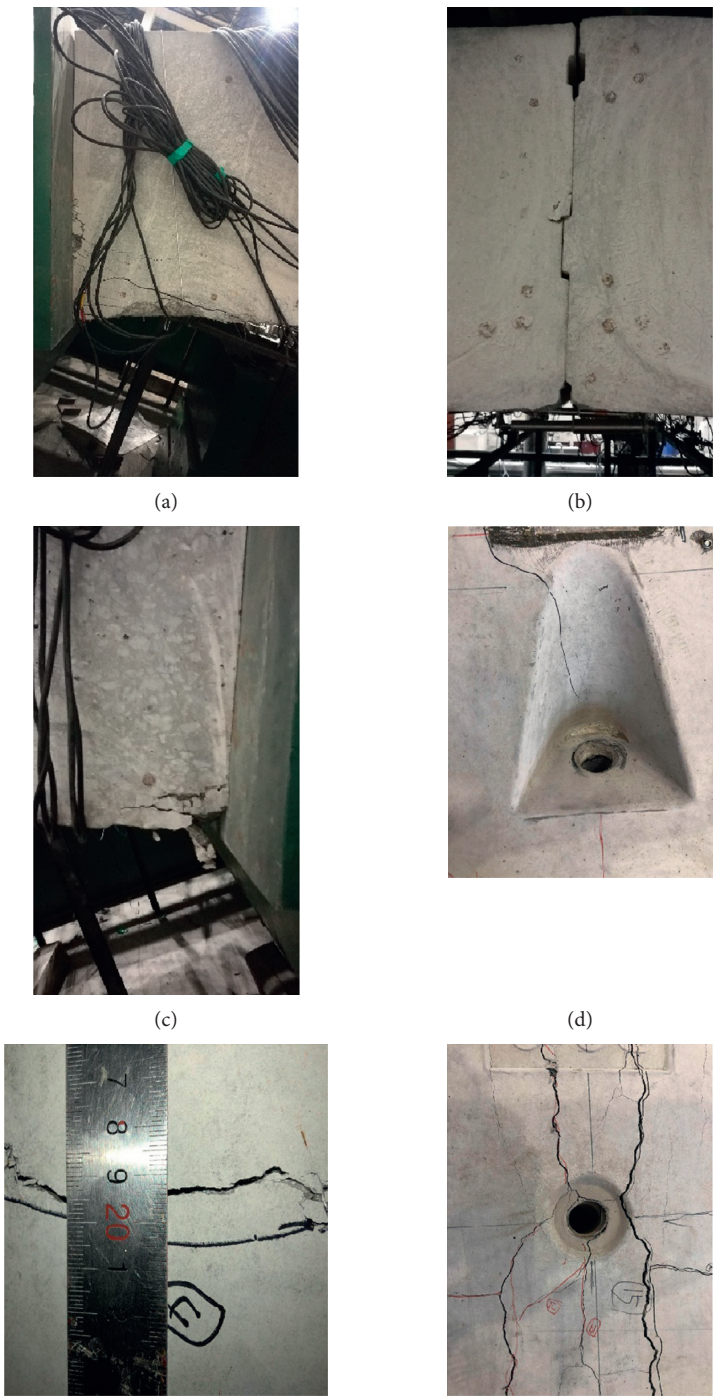

(a) (b) (c) (d) (e) (f)

Figure 14: Continued.

(g)

(h)

(i)

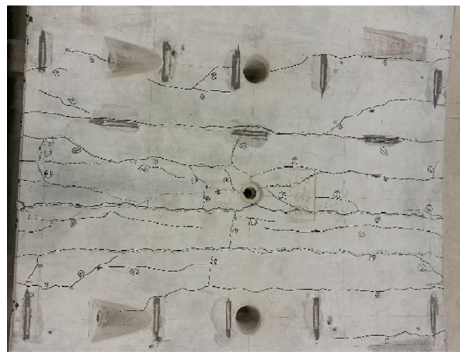

(j)

(k)

Figure 14: Continued.

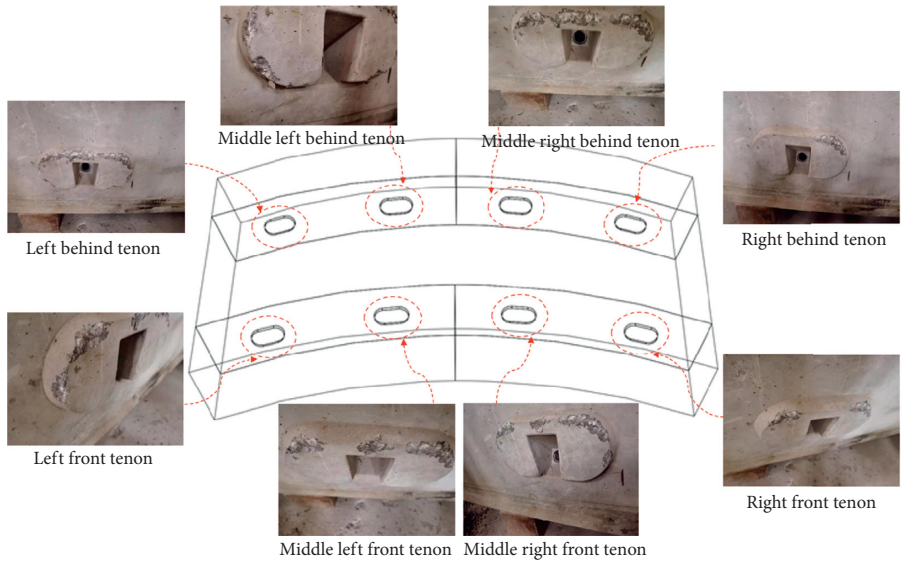

Figure 14: Final broken shape of the intermediate ring segment: (a) damaged in left inner corner, (b) local failure of longitudinal joints, (c) failure of the right inner corner, (d) bolt hole crack, (e) longitudinal crack, (f) cracks around the grouting hole, (g) partial failure of the left lateral longitudinal joint, (h) outside the vault collapsed, (i) local failure of the outer longitudinal joint on the right, (j) schematic diagram of the internal crack, (k) schematic diagram of cracks in thickness direction, and (l) the damage of mortises and tenons.

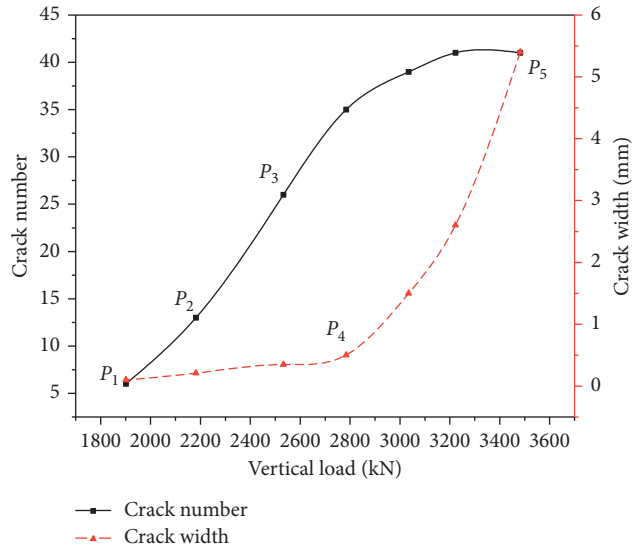

Figure 15: Variation of the number and width of cracks.

entirely penetrated) appear ⟶ the number of cracks increased rapidly. Oblique cracks appeared in the positioning holes and the bolt holes ⟶ the inner arc surface steel bar began to yield ⟶ the structure deformed significantly, and the joints opened obviously ⟶ the width of the inner arc surface through cracks increased rapidly ⟶ the load remained unchanged, and the vertical displacement continued to increase, followed by structural instability and failure.

The failure mechanism of this test is that when the assembled segments are subjected to a large load, the inner concrete of the control section reaches the ultimate tensile strain first and cracks. After the cracks appear in the segment, the stiffness of the structure of the middle ring segment decreases, and the overall rigidity of the assembled segments is redistributed, resulting in the redistribution of internal forces and deformations in the structure. Then, the concrete in the region of greater rigidity reached the limit state again and cracked. Subsequently, the process continued according to the above rules until the overall structural rigidity of the assembled segments was reduced to a certain level. Finally, while the load remained unchanged, the vertical displacement of the segment continued to increase, and the structure is damaged and unstable. The failure form

Table 1: The relationship between crack development and structural mechanical properties.

Feature points	Fracture	Maximum crack width (mm)	Maximum fracture length (mm)	Maximum opening (mm)	Bending moment (kN m)	Deformation (mm)	Maximum reinforcement strain ($\mu\varepsilon$)	Eccentric distance (m)
P_1	Visible cracks appear	0.1	708	0.402	648	7.23	229	0.341
P_2	The crack width reaches the limit	0.21	2000	0.513	802	8.62	267	0.343
P_3	The number of cracks is increasing rapidly	0.35	2000	0.811	931	11.47	611	0.345
P_4	Crack width increases rapidly	0.5	2000	1.197	1214	14.66	985	0.450
P_5	Structural failure	5.4	2000	6.914	1922	45.65	2023	0.713

of this test was compression-bending failure. There was a small number of diagonal cracks, and they were distributed mainly near the bolt holes, positioning holes, and grouting holes. It is apparent that the presence of the corners in these areas caused the concentration of the local stress in the segments. There was a certain angle between the direction of the principal stress and the longitudinal axis of the tunnel, resulting in oblique cracks in the principal stress direction of these areas.

The width of the cracks on the surface of the arc in the segment and the vertical displacement of the vault were used as the safety evaluation indices of the segment in the failure stage. In this project, the widths of the cracks began to grow rapidly after the P4 node, and the growth continued until the structure of the P5 node failed. It generally is believed that the rapid growth of the widths of the cracks is a precursor to failure. Therefore, when the vertical load reached 3035 kN, it was safe to choose various indices between P4 and P5 as the safety evaluation standard of this project. Specifically, the maximum width of a crack was 1.5 mm, the vertical displacement of the control section was 21.21 mm, and the displacement was equal to 1.62% of the diameter of the segment. When the deformation of the tunnel structure reaches any index between the two, corresponding measures should be taken immediately to prevent structural failure.

5. Conclusions

In this paper, a failure test of the prototype segment structure was conducted considering the staggered joint assembly and distributed mortises and tenons. The mechanical characteristics and crack propagation law of the segment structure during the failure process were studied, resulting in the following main conclusions:

(1) N-M curve can be applied for the evaluation of internal force; it was concluded that the segments with mortises and tenons involved large eccentric failure and that the ultimate bearing capacity is $M = 1993$ kN m, where $N = 2{,}700$ kN.

(2) According to the vertical displacement change law, the failure process of the segment is divided into three stages, that is, the elastic stage, the elastoplastic stage, and the plastic stage, and it is recommended that the single-point displacement limit index of segments with mortises and tenons be reduced to be between 1.5% and 1.8%. The overall displacement distribution of the segment structure has the shape of a funnel, with large dome displacement and small displacement on both sides.

(3) Limit use for longitudinal joint opening is suggested to be less than 3 mm for the segments with mortises and tenons, and the damage degrees of tenons are not identical for different points of tenons. The changing law of the longitudinal joint opening of the segment can be divided into three stages, that is, slow increase, accelerated increase, and sharp increase. The change process of the inner main reinforcement can be divided into two stages, that is, linear change and nonlinear change. The maximum tensile strain of the main reinforcement reaches the yield state. The outer main reinforcement had a linear growth law, and the maximum compressive strain was $-844\,\mu\varepsilon$, which was less than the yield state.

(4) The width of structural cracks and the vertical displacement of the control section can be used as safety evaluation indicators. The rapid growth of the widths of the cracks is a precursor to failure. Specifically, the

maximum width of the cracks was 1.5 mm, and the vertical displacement of the control section was 21.21 mm (about 1.62% of the diameter of the segment). When either one of these two conditions is reached, it can be considered that the structure is about to fail, and corresponding protective measures must be taken immediately.

Data Availability

The data used to support the findings of this study are available from the corresponding author upon request.

Conflicts of Interest

The authors declare that there are no conflicts of interest regarding the publication of this paper.

References

[1] J. Liu and X. HOU, *Shield Tunneling*, p. 3, China Railway Publishing House, Beijing, China, 1991.

[2] C. He and B. Wang, "Research progress and development trends of highway tunnels in China," *Journal of Modern Transportation*, vol. 21, no. 4, pp. 209–223, 2013.

[3] H. Zhang, *Numerical Simulation of the Impact of Shield Tunneling on the Surrounding Environment*, Hohai University, Nanjing, China, 2005.

[4] Y. Tang, *Longitudinal Stress Analysis of Tube Lining of Complex Underwater Shield Tunnel under Special Circumstances*, Southwest Jiaotong University, Chengdu, China, 2017.

[5] M. Xiao, F. Kun, and C. Li, "Research on the calculation method of surrounding rock pressure of shield tunnel in composite formation," *Journal of Rock Mechanics and Engineering*, vol. 38, no. 9, pp. 1836–1847, 2019.

[6] C. He, F. Kun, and Q. Yan, "Research on the distribution law of internal force of underwater shield tunnel slices in high-speed railway," *Journal of Railways*, vol. 34, no. 4, pp. 101–109, 2012.

[7] Z. Yan, Y. Peng, and W. Ding, "Load test research on single layer lining pipe joint of water conveyance tunnel of Qingxinsha water source," *Journal of Geotechnical Engineering*, vol. 33, no. 9, pp. 1385–1390, 2011.

[8] Y. Qiu, C. He, and F. Kun, "Local prototype structure loading test of shield tunnel segment lining effect," *Chinese Journal of Highways*, vol. 30, no. 8, pp. 156–163 + 215, 2017.

[9] F. Kun, C. He, and Y. Zou, "Study on the effect of the pipe segment assembly method on the internal force of large-section tunneling shield tunneling," *Engineering Mechanics*, vol. 29, no. 6, pp. 114–124, 2012.

[10] F. Kun, C. He, and Z. Su, "Nanjing Yangtze river tunnel tube lining structure prototype loading test," *Journal of China Highway*, vol. 26, no. 1, pp. 135–143, 2013.

[11] C. He, F. Kun, and Q. Yan, "Research on the prototype loading test of the subsea shield tunnel segment lining structure," *China Engineering Science*, vol. 14, no. 10, pp. 65–72+89, 2012.

[12] Y. Qiu, F. Kun, and C. He, "Failure test of local prototype structure of staggered and piecework pipe lining of shield tunnel," *Chinese Journal of Civil Engineering*, vol. 52, no. 4, pp. 98–108, 2019.

[13] F. Kun, C. He, and Z. Su, "Experimental study on structural failure of Nanjing Yangtze river tunnel prototype," *Journal of Southwest Jiaotong University*, vol. 46, no. 4, pp. 564–571, 2011.

[14] K. Liang, F. Kun, and S. Xiao, "Effect of the position of the top sealing block on the structure of the high-water pressure through-joint assembled pipe segment [J/OL]," *Journal of Southwest Jiaotong University*, vol. 1–9, 2020.

[15] S. Xia, *Prototype Experimental Study on the Slits Lining Structure of Liyang Tunnel*, Southwest Jiaotong University, Chengdu, China, 2010.

[16] B. Xiangli, X. Liu, and X. Wang, "Full scale test study on the ultimate bearing capacity of shield tunnel structure reinforced by inner tensile steel ring," *Chinese Journal of Civil Engineering*, vol. 47, no. 11, pp. 128–137, 2014.

[17] Y. Ye, D. Huang, and G. Li, "Experimental study on the ultimate bearing capacity of the lining structure of similar rectangular shield tunnel," *Modern Tunneling Technology*, vol. 53, no. S1, pp. 118–127, 2016.

[18] D. Lu, *Analysis on the Stress Characteristics and Crack Phenomenon of Shield Tunnel Segment during Construction*, Southwest Jiaotong University, Chengdu, China, 2019.

[19] S. Wang, J. Yao, and X. HE, "Model experimental study on the influence of water pressure on the mechanical characteristics and failure morphology of shield segment Lining," *Journal of Civil Engineering*, vol. 51, no. 4, pp. 111–120, 2015.

[20] S. Wang, X. Shen, and X. He, "Model test research on stress and failure mode of shield tunnel segment Lining under different assembly modes," *Journal of Civil Engineering*, vol. 50, no. 6, p. 114, 2017.

[21] P. Study, *On Progressive Failure Mechanism of Subsea Shield Tunnel Segment Lining Structure*, Southwest Jiaotong University, Chengdu, China, 2015.

[22] Y. Yang and X. Xie, "Research on the cracking and damage mechanism of shield tunnel segment based on fracture mechanics," *Journal of Lithology and Engineering*, vol. 34, no. 10, pp. 2114–2124, 2015.

[23] R. Park and T. Paulay, *Reinforced Concrete Structures*, Wiley, Hoboken, NJ, USA, 2009.

[24] X. Zhang, Z. Yang, and B. Hong, "Research on deformation index of shield tunnel structure health evaluation," *Underground Engineering and Tunnels*, vol. 4, no. 4, pp. 7–13 + 53, 2014.

[25] Y. Zou, *Prototype Test of Staggered Assembled Pipe Segment Lining Structure of Liyang Underwater Shield Tunnel*, Southwest Jiaotong University, Chengdu, China, 2010.